Tunable Linear and Nonlinear Optical Properties from Room Temperature Phosphorescent Cyclic Triimidazole-Pyrene Bio-Probe

Andrea Previtali,[a, b] Wei He,[c] Alessandra Forni,*[b] Daniele Malpicci,[a, b] Elena Lucenti,[b] Daniele Marinotto,[b] Lucia Carlucci,*[a] Pierluigi Mercandelli,[a] Marco Aldo Ortenzi,[a] Giancarlo Terraneo,[d] Chiara Botta,[e] Ryan Tsz Kin Kwok,[c] Jacky Wing Yip Lam,[c] Ben Zhong Tang,*[c, f] and Elena Cariati*[a, b]

Abstract: Organic materials with multiple emissions tunable by external stimuli represent a great challenge. TTPyr, crystallizing in different polymorphs, shows a very rich photophyisics comprising excitation-dependent fluorescence and phosphorescence at ambient conditions, and mechanochromic and thermochromic behavior. Transformation among the different species has been followed by thermal and X-ray diffraction analyses and the emissive features interpreted through structural results and DFT/TDDFT calculations. Partic-

ularly intriguing is the polymorph TTPyr(HT), serendipitously obtained at high temperature but stable also at room temperature, whose non-centrosymmetric structure guarantees an SHG efficiency 10 times higher than that of standard urea. Its crystal packing, where only the TT units are strongly rigidified by π-π stacking interactions while the Pyr moieties possess partial conformational freedom, is responsible for the observed dual fluorescence. The potentialities of TTPyr for bioimaging have been successfully established.

Introduction

Purely organic compounds showing room temperature phosphorescence (RTP) are receiving ever growing attention from the scientific community due to the benefits they offer, including biocompatibility and low cost, with respect to the widely used metal containing phosphorescent materials. Applications of organic RTP in several fields such as bioimaging,[1,2] anti-counterfeiting,[3,4] catalysis[5] and displays[6] have been assessed. Many strategies spanning from π-π stacking

interactions[7–9] to supramolecular approaches[10] including host-guest systems,[11,12] and co-assembly based on macrocyclic compounds,[13] crystallization[14,15] and cocrystallization,[16] halogen bonding,[17,18] and doping in a polymer matrix[19] have been developed to realize organic RTP materials. In this context, we have reported on the intriguing photophysical behavior of a family of compounds having triimidazo[1,2-a:1',2'-c:1'',2''-e][1,3,5]triazine, TT,[8] as prototype. TT is characterized by aggregation-induced emissive (AIE) behavior, displaying, in particular, ultralong phosphorescence (RTUP) (up to 1 s) under

[a] Dr. A. Previtali, Dr. D. Malpicci, Prof. L. Carlucci, Prof. P. Mercandelli, Dr. M. A. Ortenzi, Prof. E. Cariati
Department of Chemistry
Università degli Studi di Milano and INSTM RU
via Golgi 19, 20133 Milano (Italy)
E-mail: lucia.carlucci@unimi.it
        elena.cariati@unimi.it

[b] Dr. A. Previtali, Dr. A. Forni, Dr. D. Malpicci, Dr. E. Lucenti, Dr. D. Marinotto, Prof. E. Cariati
Institute of Chemical Sciences and Technologies
"Giulio Natta" (SCITEC) of CNR
via Golgi 19, 20133 Milano (Italy)
E-mail: alessandra.forni@scitec.cnr.it

[c] Dr. W. He, Prof. R. T. K. Kwok, Dr. J. W. Y. Lam, Prof. B. Z. Tang
Department of Chemistry
Hong Kong Branch of Chinese National Engineering Research Center for Tissue Restoration and Reconstruction
The Hong Kong University of Science and Technology
Clear Water Bay, Kowloon, Hong Kong (China)

[d] Prof. G. Terraneo
Laboratory of Supramolecular and Bio-Nanomaterials (SupraBioNanoLab)
Department of Chemistry, Materials, and Chemical Engineering
"Giulio Natta" Politecnico di Milano
via Mancinelli 7, 20131 Milano (Italy)

[e] Dr. C. Botta
Institute of Chemical Sciences and Technologies
"Giulio Natta" (SCITEC) of CNR
via Corti 12, 20133 Milano (Italy)

[f] Prof. B. Z. Tang
Shenzhen Institute of Molecular Aggregate Science and Engineering
School of Science and Engineering
The Chinese University of Hong Kong
Shenzhen, 2001 Longxiang Boulevard, Longgang District
Shenzhen City, Guangdong 518172 (P. R. China)
E-mail: tangbenz@ust.hk

Supporting information for this article is available on the WWW under
https://doi.org/10.1002/chem.202102839

Chemistry–A European Journal

Full Paper
doi.org/10.1002/chem.202102839

Chemistry Europe
European Chemical
Societies Publishing

ambient conditions associated with the presence of strong π-π stacking interactions in the crystalline structure.[7] The presence of one or multiple heavy (Cl, Br and I) atoms on the TT scaffold greatly modifies both its molecular and solid state photophysical behavior resulting in a complex excitation dependent photoluminescence with emissions comprising dual fluorescence, molecular phosphorescence, supramolecular RTP and RTUP, covering a wide portion of the visible region.[9,20–22] The introduction of chromophoric fragments, namely 2-fluoro-pyridine and 2-pyridine (TT-py), has provided increased molecular performances with respect to TT itself, comprising fluorescence and heavy atom free phosphorescence, preserving the solid state RTUP which is shifted to the red with respect to the TT parent compound.[23,24] In particular, a detailed study on TT-py polymorphs has allowed to disclose the role of the partial mobility of the pyridinic fragment in the observed dual fluorescence of the crystalline compounds.[24]

The development of novel advanced luminescent materials could boost the exploration in life science. The materials contribute to reveal the underlying operating rules and extend our understanding towards various biological systems, eventually shedding light on the "black box" that precisely regulates sophisticated life processes.[25] The new era for life science started in 1882 when Paul Ehrlich used the fluorescent dye uranin to determine the pathway of secretion of aqueous humour in the eye.[26] The technique for labeling antibodies with fluorescent dyes developed by Albert Coons in 1940s gave birth to the field of immunofluorescence. The introduction of green fluorescent protein (GFP) has allowed systematic imaging studies of protein localization in living cells and of the structure and function of living tissues.[27] Afterwards, the development of activable fluorescent probes accelerated the progressing of super resolution microscopy,[28] unrevealing the mysterious cellular world beyond the optical limiting.[29] Especially, the emergence of delayed fluorescent materials and RTP materials opened an alternative path for life science research. The autofluorescence in living systems could be avoided by virtue of long-lived emission.[30–32] The relative time-resolved imaging techniques expanded the application range of biological systems. Thereinto, RTUP materials attracted abundant attention for advanced bioapplications. Moreover, the development of aggregate materials with emission tunability and coexistence of multiple radiative behaviors is a burgeoning area where highly potential applications could be explored.[33,34]

Here we report on the preparation and characterization of different solvated (namely TTPyr(Et) and TTPyr(Me)) and not solvated (TTPyr(RT) and TTPyr(HT)) solid phases of 3-(pyren-1-yl)triimidazo[1,2-*a*:1′,2′-*c*:1″,2″-*e*][1,3,5]triazine hereafter TTPyr. The thermally induced structural transformation (from TTPyr(Et) to TTPyr(HT) through TTPyr(RT)) among the phases involves bright and tunable prompt and long-lived emissions as well as NLO (nonlinear optical) properties switched on by the packing features of the chromophore. Phase transformation has been followed by optical, thermal and X-ray diffraction studies. Detailed photophysical investigation on TTPyr solutions, films and crystals reveals that RTP is enhanced through intermolecular interactions; packing features and crystals size are funda-

mental in modulating both the prompt and the long-lived components. Moreover, the material in aggregate-state has been exploited for bioimaging applications, including its potential cellular imaging and bacterial imaging.

Results and Discussion

TTPyr can be synthetized in high yields by Suzuki coupling reaction between mono-brominated TT1Br[9] and the corresponding boronic acid derivative and further purified by standard chromatography techniques and crystallization.

TTPyr crystallizes in three different forms, namely TTPyr(RT), TTPyr(Et) and TTPyr(Me), by slow diffusion, in a DCM solution of the chromophore, of non-solvents hexane, EtOH and MeOH, respectively. While crystals of TTPyr(RT) and TTPyr(Et) are suitable for an accurate X-ray diffraction analysis (Figures 1 and 2, respectively), the quality of TTPyr(Me) crystals is not sufficient to establish a fully refined model, possibly due to the fast loss of methanol molecules at room temperature. However, a tentative solution for this species, showing similarities to the TTPyr(RT) phase, is reported in the Supporting Information.

TTPyr(RT) crystallizes in the monoclinic $P2_1/c$ space group with one molecule in the asymmetric unit, while crystals of TTPyr(Et) belong to the $C2/c$ monoclinic space group. The asymmetric unit of the latter structure contains one TTPyr molecule and half ethanol molecule which is disordered over two positions, allowing it to interact one by one through hydrogen bond with two TTPyr units (O—H···N = 3.261(8) Å) (Figure 2).

Molecules of TTPyr are characterized by similar values of dihedral angle (θ) between the Pyr and TT mean planes (θ = 49.31(3)° and 46.79(3)° in TTPyr(RT) and TTPyr(Et), respectively). The bond connecting the TT and Pyr units measures 1.476(2) (TTPyr(RT)) and 1.470(2) Å (TTPyr(Et)). In TTPyr(RT) the triimida-
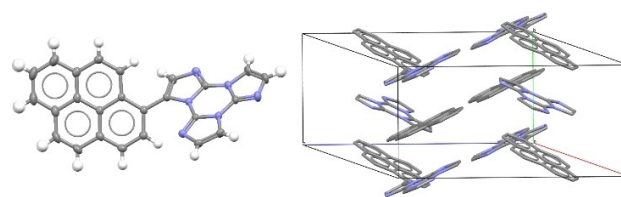

Figure 1. X-ray crystal structure of TTPyr(RT). Left: view of a single TTPyr molecule (ellipsoid drawn at 30%); right: view of molecular packing (hydrogen atoms are omitted for clarity).
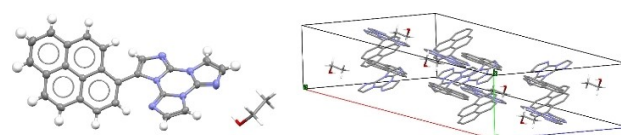

Figure 2. X-ray crystal structure of TTPyr(Et). Left: view of a single TTPyr molecule interacting through hydrogen bond with an ethanol molecule (ellipsoid drawn at 30%, only one model of disordered ethanol molecule is shown); right: view of the molecular packing (hydrogen atoms are omitted for clarity and only one model is shown for ethanol molecules).

Chemistry–A European Journal

Full Paper
doi.org/10.1002/chem.202102839

Chemistry
Europe
European Chemical
Societies Publishing

zole unit of one molecule stacks in between two Pyr units of neighbour molecules, with distances of 3.802(2) and 4.033(2) Å between triazine and pyrene centroids, forming infinite columns of π-π stacking fragments (Figure 1). This arrangement is unusual for the reported members of the TT-family, all having stacking interactions between TT-units of adjacent molecules[8,9,20–24] and represents an interesting case of study for the photophysical behavior associated with the presence of π stacking arrangements. In TTPyr(Et), TTPyr molecules align in antiparallel fashion along the crystallographic **b** direction giving rise to columns similar to those found in the crystal structure of TTPyr(RT). Along these columns, TT and pyrene fragments stack in parallel arrangement with alternating distances of 3.780(2) and 3.978(2) Å between triazine and pyrene centroids (Cg). The Cg···Cg separations are therefore slightly shorter in TTPyr(Et) with respect to TTPyr(RT).

Intriguingly, in the attempt to thermally prepare a sample of TTPyr(Me) of better diffraction quality, crystals of a new phase were obtained. In particular, crystals of TTPyr(HT) were isolated by maintaining overnight a microcrystalline sample of the methanol solvate phase at temperature few grades below its melting point (m.p. = 232 °C) and successively slowly cooling (0.2 °C/min) to room temperature.

TTPyr(HT) crystallizes in the orthorhombic $Pna2_1$ space group with one molecule in the asymmetric unit (Figure 3). The dihedral angle between mean planes of TT and pyrene is 52.78(6)°, slightly larger with respect to that found for its room temperature polymorph TTPyr(RT). The packing is completely different from that found for TTPyr(RT). The molecules form columns along the crystallographic **a** direction and only the TT fragments are facing each other, while the pyrene units of adjacent molecules protrude in opposite directions. Along the columns, the mean planes of two adjacent TT units are not parallel, showing a dihedral angle of 8.22(3)°. The distance between triazine centroids of adjacent TT fragments along the crystallographic **a** direction is 4.111(4) Å.
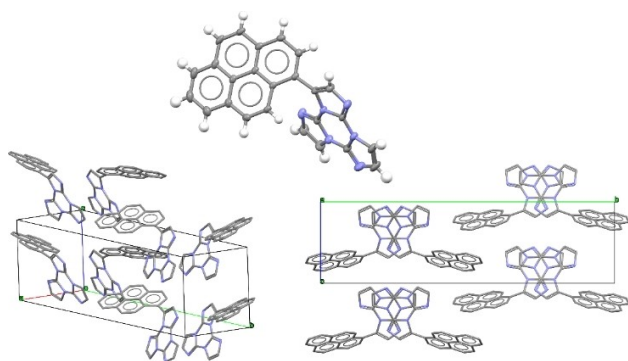

Figure 3. X-ray crystal structure of TTPyr(HT). Top center: view of a single TTPyr molecule (ellipsoids are drawn at 30%); bottom: two views of the molecular packing (hydrogen atoms are omitted for clarity).

Thermal behavior

To study the thermal behavior of the solvated species TTPyr(Et) and characterize its conversion to the de-solvated species TTPyr (RT) and TTPyr(HT), DSC and TGA (Figure S5) and VT-XRPD (variable temperature X-ray powder diffraction, Figure S6) were performed on freshly prepared crystalline samples. The TGA trace shows that the sample starts to lose weight only at temperature higher than 170 °C (b.p. of ethanol 79 °C), explaining the much higher stability of the ethanol solvate crystals with respect to that of the methanol containing phase.

The DSC analysis displays a first endothermic transition at 166 °C (ethanol loss) and a second one at 233 °C (melting of the desolvate phase) followed by an exothermic transition at 241 °C (crystallization to the TTPyr(HT) crystal phase). Heating/cooling cycles in DSC evidence that the transformation of TTPyr(RT) in TTPyr(HT) is irreversible.

The thermal transformation of TTPyr(Et) into TTPyr(RT) and successively into TTPyr(HT) performed by VT-XRPD experiment is reported in Figures S6 and S7. TTPyr(Et) starts to give TTPyr (RT) at 140 °C, while the formation of TTPyr(HT) begins at 220 °C (Figure S6).

Based on thermal and XRPD results, pure TTPyr(HT) samples were prepared starting from either TTPyr(RT), TTPyr(Me) or TTPyr(Et) by heating at 220 °C for at least 30 minutes in air. Moreover, since TTPyr(HT) phase crystallizes in a non-centro-symmetric space group, which is a strict requirement to have non-zero second order nonlinear optical (NLO) properties, its second harmonic generation (SHG) response was evaluated with a Kurtz-Perry setup at 1064 nm non resonant wavelength.[35] By comparison with standard urea powders, its SHG response resulted 10 times higher, indicating an efficient packing of the chromophore in the crystal structure. This good performance, together with the material optical transparency, suggest its further implementation in the NLO field.

Photophysical characterization

TTPyr in different phases was characterized by steady state and time resolved spectroscopy (Table 1). Diluted DMSO solutions of TTPyr (10^{-5}–10^{-6} M) show at room temperature (RT) two absorptions with peaks at 257, 268, 279 nm (ES$_2$) and 332, 347 nm (ES$_1$) respectively, and an intense very broad fluorescent emission at 420 nm (quantum yield, Φ, equal to 92%) (Figures 4 and S8). Spin-coated blended films of TTPyr in polymethylmethacrylate (PMMA) (0.5 wt% and 5 wt%) show an intense, vibronically resolved fluorescence at 396 nm (Φ about 75%) and excitation maxima at 277 and 344 nm (Figures 4 and S9).

Absorption peaks in solution and PMMA films are ascribed to transitions of main pyrene character, as suggested by the similarity with the absorption spectrum of pyrene itself in the same conditions, showing peaks at 254, 264, 274 nm and 309, 322, 338 nm (Figure S10).

The interpretation of the different emissive behavior displayed by TTPyr in solution or in blended films is trickier than absorption. DFT analysis of the potential energy surface

Table 1. Photophysical parameters of TTPyr phases.

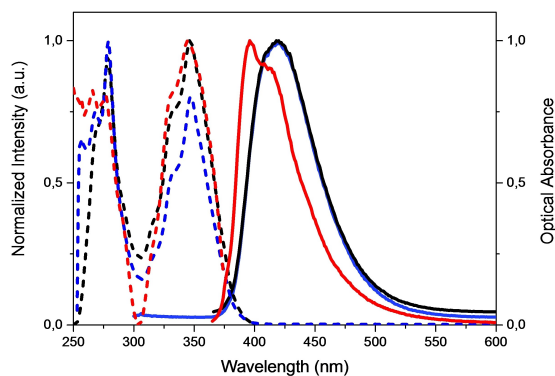| TTPyr			298 K Φ [%]	λ$_{em}$ [nm]	τ$_{av}$	77 K λ$_{em}$ [nm]	τ$_{av}$
DMSO (10^{-5} M)			92	420	2.76 ns		
DMSO/H$_2$O 10/90 v/v (10^{-5} M)			68	395	12.32 ns		
				475	25.66 ns		
Amorphous film				465	9.32 ns		
				531			
Pristine cast film			50	470	6.95 ns		
				510	4.78 ms		
Cast film heated at 220°C			12	459	1.73 ns		
				530	13.63 ms		
Blended PMMA film (0.5–5%)			75	396			
TTPyr(Et)			53	493	2.97 ns	463, 493, 520	4.17 ns
				555	4.95 ms	553, 596	5.37 ms
TTPyr(Me)			42	499	3.38 ns		
				550	5.18 ms		
TTPyr(RT)	Small crystal		38	490	3.03 ns		
				550	4.54 ms		
	Large crystal		20	490	1.85 ns	463, 492, 520	2.66 ns
				550	4.62 ms	556, 599	5.61 ms
	Ground crystal		54	475	2.15 ns	462, 488	3.93 ns
				514	5.19 ms	517, 553	5.76 ms
TTPyr(HT)	from TTPyr(Et)		21	420, 447		415, 437	
				487		487	
				530		540, 576	
	from TTPyr(RT)	Small crystal		422, 443			
				483			
				524, 563			
		Large crystal	21		0.62 ns	413, 450	1.56 ns
				480	1.99 ns	478	2.91 ns
				549	23.4 ms	553, 590	26.2 ms
		Ground crystal		459	0.71 ns		
					3.46 ns		
				567	3.70 ms		

Figure 4. TTPyr in DMSO solution and PMMA film. DMSO solution 10^{-5} M at RT: normalized emission at $λ_{exc} = 280$ nm (blue full line); $λ_{exc} = 346$ nm (black full line); normalized excitation at $λ_{em} = 420$ nm (black dashed line); normalized absorption (blue dashed line). In PMMA (5% w/w) at RT: normalized emission at $λ_{exc} = 345$ nm (red full line), normalized excitation $λ_{em} = 397$ nm (red dashed line).

(PES) of the isolated 'gas-phase' chromophore (Figure 5) reveals the presence of two conformational minima in a very flat region, corresponding to different orientation of pyrene with respect to the TT moiety, as denoted by the C1-C2-C10-C11 torsion angle, $τ$ (Figure S4). The more stable conformation (S$_{0,HT}$), having optimized torsion angle $τ_{opt} = 67.4°$, is found in the crystal structure of TTPyr(HT) ($τ_{cryst} = 48.8(5)°$), while the other (S$_{0,RT}$, $τ_{opt} = 110.3°$), less stable by only 0.6 kcal/mol, is observed in TTPyr(Et) and TTPyr(RT) ($τ_{cryst} = 129.52(19)$ and $128.47(18)°$, respectively). TDDFT determination of the electronic levels of TTPyr in the two minima provides essentially the same set of excitation energies (Table S6), consisting in two lower energy transitions, S$_1$ (at 304 nm) and S$_2$ (at 302 nm), a very weak intermediate transition, S$_3$ (at 249 or 251 nm for the two conformations) and a strong transition, S$_4$, at high energy (237 nm). In agreement with the observed absorption spectrum, all the transitions mainly involve molecular orbitals localized on the pyrene moiety with only a small contribution (coming from HOMO-1) on TT (Table S6 and Figures S56, S57). Moreover, the energetic separation between the strongly allowed transitions S$_4$ and S$_1$ (HT conformation) or S$_2$ (RT conformation), about 1.10 eV, matches with good approximation the observed ES$_2$–ES$_1$ energy gap (0.94 eV). Optimization of the S$_1$ state in the two conformations leads in both cases to a much less twisted geometry with respect to the ground state, $τ_{opt}$ varying from 67.4 to 41.5° (S$_{1,HT}$) and from 110.3 to 138.5° (S$_{1,RT}$), with shortening of the bond connecting the TT and Pyr units (from 1.478 to 1.435 and 1.425 Å, respectively), implying a greater conjugation between them. Emission from both relaxed S$_1$ states is computed at 370 (S$_{1,HT}$) and 384 nm (S$_{1,RT}$), respectively,
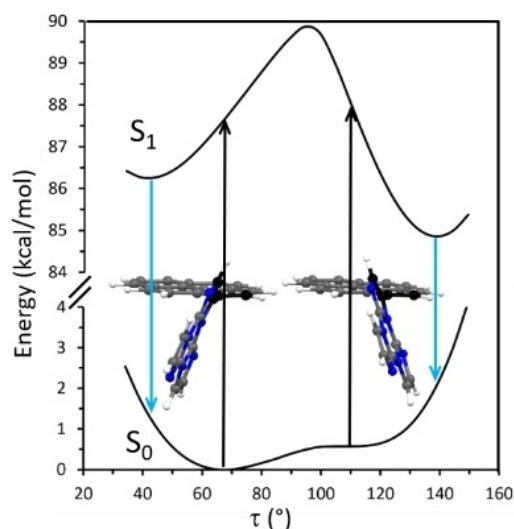
Chemistry–A European Journal

Full Paper
doi.org/10.1002/chem.202102839

Chemistry Europe
European Chemical
Societies Publishing

Figure 5. Scan of the relaxed potential energy surface of the S_1 and S_0 states of TTPyr along the C1-C2-C10-C11 torsion angle τ (atoms in black) at the (TD)-ωB97X/6-311++G(d,p) level of theory. The optimized $S_{0,HT}$ (left) and $S_{0,RT}$ (right) conformations are reported together with the corresponding absorption and emission paths (black and cyano arrows, respectively). Energies are relative to the $S_{0,HT}$ equilibrium geometry.

and involves HOMO and LUMO both delocalized on pyrene with a large tail on TT.

Owing to the flatness of the S_0 PES around the two minima, both conformations are populated in diluted solution, resulting in a broad fluorescent emission. On the other hand, in PMMA the chromophore is frozen in the absolute minimum, $S_{0,HT}$, and a narrower higher energy emission is observed.

The effect of interchromophoric interactions on the emissive behavior of the compounds can be determined through solid state investigation both on crystals/powders and neat films. Owing to the polymorphic behavior of TTPyr, and in particular the very different crystalline arrangement of the dye in TTPyr (HT) with respect to the other phases, investigation on the photophysical properties in solid state appears highly relevant. In agreement with the similarity of the chromophore's disposition inside the structure, crystals of TTPyr(RT), TTPyr(Et) and TTPyr(Me) display similar photophysical behavior (Φ about 40%), comprising one fluorescence (at 491, 493 and 499 nm, respectively) and one phosphorescence (549, 555 and 550 nm, respectively) (Table 1, Figures 6 and S11–S17), this latter detectable only by exciting at low energy. Moreover, the three compounds display almost superimposable excitation spectra.

It is however to be noted that the relative intensity of fluorescence and phosphorescence seems to depend on the crystals size of the examined samples. To better investigate this aspect, we have photophysically characterized two batches of TTPyr(RT) containing crystals of macroscopically different dimensions (TTPyr(RT)-small and TTPyr(RT)-large, Figure 7 left and right, respectively). When comparing the two emissive behaviors, it appears that the dimensions of the crystals play a role in the relative intensities of the two bands. In particular, by exciting at 300 nm, a reduced fluorescence contribution is observed for TTPyr(RT)-large. Accordingly, shorter fluorescence lifetimes (from 3.03 to 1.85 ns for TTPyr(RT)-small and TTPyr(RT)-large, respectively, Figures S18 and S20) are measured indicating easier intersystem crossing (ISC). Moreover, a decrease in the overall quantum efficiency (from 38% for TTPyr(RT)-small to 20% for TTPyr(RT)-large) is observed. An increased autoabsorption phenomenon for large crystals can be excluded based on the small excitation-emission spectral overlap and the reported lifetimes. Moreover, an easier triplet population for large crystals is also supported by a singlet-triplet excitation peak of sizable intensity at about 480 nm.

The effect of crystal dimensions on emissive features was further investigated through spectra collected for crystals of TTPyr(RT)-large ground in an agate mortar (Figure S25). A clear intensification of the high energy component at about 480 nm and an enhancement of the quantum yield (54%) are observed. It has also to be noted that an additional higher energy fluorescence (420 nm) can be recognized as a very weak
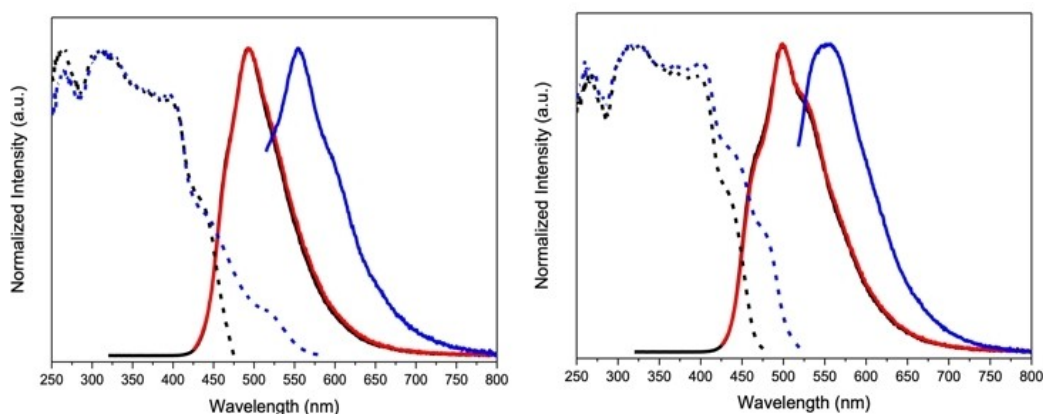

Figure 6. Normalized emission (full line) and excitation (dashed line) spectra at RT. Left: TTPyr(Et) crystals. $\lambda_{exc}=300$ nm (black line), $\lambda_{exc}=405$ nm (red line), $\lambda_{exc}=495$ nm (blue line); $\lambda_{em}=494$ nm (black line); $\lambda_{em}=610$ nm (blue line). Right: TTPyr(Me) crystals. $\lambda_{exc}=300$ nm (black line), $\lambda_{exc}=405$ nm (red line), $\lambda_{exc}=498$ nm (blue line); $\lambda_{em}=498$ nm (black line); $\lambda_{em}=550$ nm (blue line).

Chemistry–A European Journal

Full Paper
doi.org/10.1002/chem.202102839

Chemistry
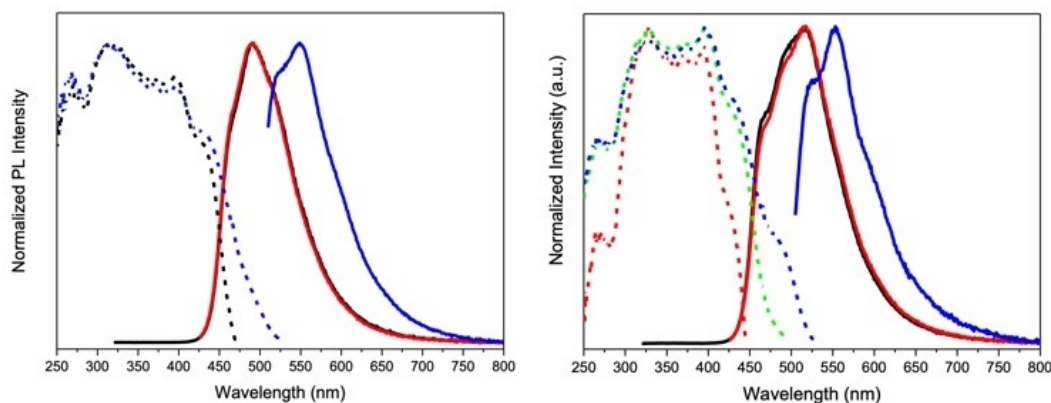Europe
European Chemical
Societies Publishing

Figure 7. Normalized emission (full line) and excitation (dashed line) spectra of TTPyr(RT)-small (left) and TTPyr(RT)-large (right) crystals at RT. $\lambda_{exc} = 300$ nm (black line), $\lambda_{exc} = 405$ nm (red line), $\lambda_{exc} = 490$ nm (blue line); $\lambda_{em} = 490$ nm (black line), $\lambda_{em} = 555$ nm (blue line), $\lambda_{em} = 466$ nm (red line), $\lambda_{em} = 513$ nm (green line).

component in spectra of TTPyr(RT)-ground collected at 77 K (Figures S28 and S29).

Intriguingly, TTPyr(HT), having peculiar crystal structure, displays a macroscopically different photophysical behavior with respect to the other three phases of TTPyr. At room temperature, polycrystalline samples of TTPyr(HT) show two fluorescences and one phosphorescence (Figures 8, 9 and S32–S40). The presence of the three emissions represents a reproducible finding, however their relative intensity depends

Figure 8. Images (bar size 50 μm) taken with a fluorescence microscope of a single crystal of TTPyr(Et) at a) 20 °C, b) 180 °C, c) after 30 min at 220 °C, d) after cooling down at 20 °C; bottom: PL spectra before (black line) and after thermal treatment (blue line), $\lambda_{exc} = 350$ nm.

on the particular batch. As reported above, TTPyr(HT) can be prepared by heating at 220 °C for at least 30 min any of the crystal phases of TTPyr as confirmed by XRPD patterns. Therefore, to get a complete view of the photophysical behavior of TTPyr(HT), we spectroscopically characterized three batches obtained by heating TTPyr(Et), TTPyr(RT)-small and TTPyr(RT)-large crystals. In particular, the thermal transformation from TTPyr(Et) to TTPyr(HT) was followed by a fluorescence microscope. Images taken at selected temperatures (Figure 8) indicate that, while the shape and size of the starting crystals are preserved, a gradual loss of transparency occurs, confirming that no single crystal-to-single crystal process is taking place.

Spectra recorded for TTPyr(HT) obtained from TTPyr(Et) (two batches), TTPyr(RT)-small and TTPyr(RT)-large crystals are reported in Figures 8 (bottom) and 9. A high energy fluorescence with peaks at 420 and 450 nm, a low energy fluorescence, with maximum at 480 nm and one phosphorescence at 550 nm are clearly identified. As mentioned above, their relative intensity varies and depends on the excitation energy. The high energy fluorescence, hardly visible in the room temperature spectrum of TTPyr(HT) obtained from TTPyr(RT)-large crystals, becomes visible when recording the spectrum at 77 K (Figure S37). At this temperature, all emissive components acquire a better vibronic resolution. Moreover, by grinding TTPyr(HT) obtained from TTPyr(RT)-large crystals, a macroscopic change of the emission spectrum is observed (Figure S41). In particular, the high energy fluorescence (almost the only present) becomes predominant by exciting at high energy with lifetimes almost unaffected by the grinding process (0.62 and 0.71 ns for unground and ground TTPyr(HT), respectively). On the contrary, lifetimes of the low energy fluorescence are prolonged in the ground sample (1.99 and 3.46 ns for unground and ground TTPyr(HT), respectively) and those of the long-lived component are macroscopically reduced (23.4 and 3.7 ms for unground and ground TTPyr(HT), respectively). These results suggest that the triplet state can be more easily populated and is more stabilized in the unground samples. It has also to be mentioned that, based on the small Stokes shift of the high energy fluorescence,
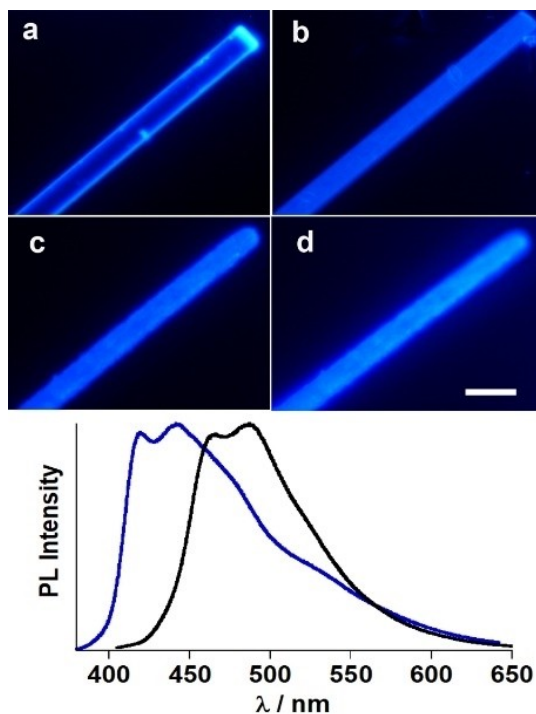
Chemistry–A European Journal

Full Paper
doi.org/10.1002/chem.202102839

**Chemistry
Europe**
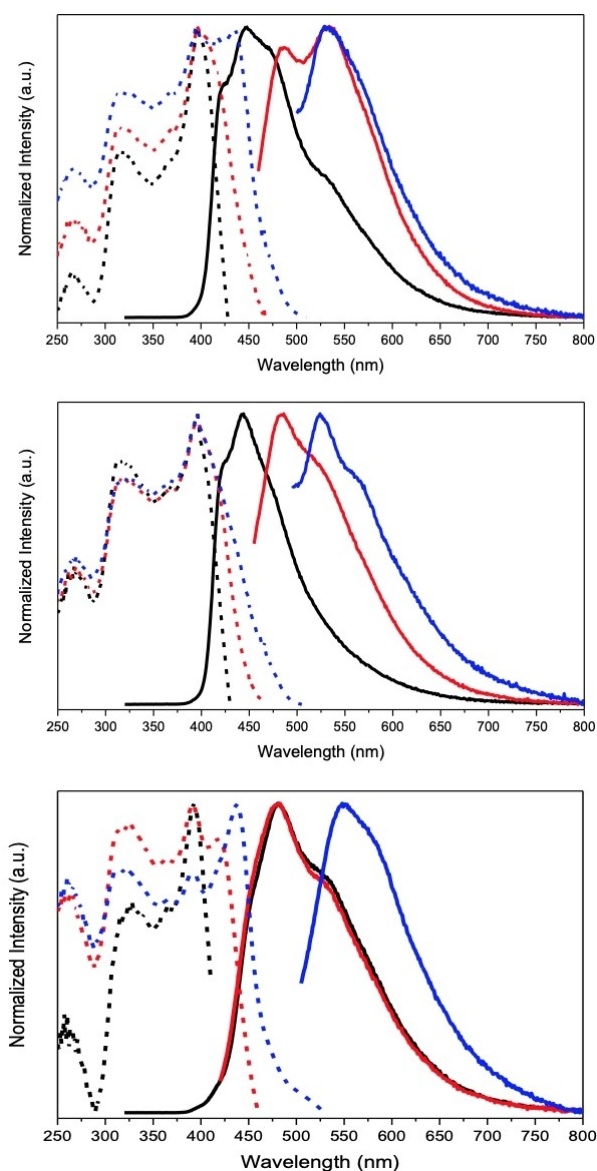European Chemical
Societies Publishing

Figure 9. Normalized emission (full line) and excitation (dashed line) spectra of TTPyr(HT) polycrystalline samples obtained from crystals of TTPyr(Et) (top), TTPyr(RT)-small (centre) and TTPyr(RT)-large (bottom) at RT. Top: $\lambda_{exc} = 300$ nm (black line), $\lambda_{exc} = 440$ nm (red line), $\lambda_{exc} = 486$ nm (blue line); $\lambda_{em} = 448$ nm (black line), $\lambda_{em} = 487$ nm (red line), $\lambda_{em} = 534$ nm (blue line). Centre: $\lambda_{exc} = 300$ nm (black line), $\lambda_{exc} = 440$ nm (red line), $\lambda_{exc} = 480$ nm (blue line); $\lambda_{em} = 445$ nm (black line), $\lambda_{em} = 483$ nm (red line), $\lambda_{em} = 524$ nm (blue line). Bottom: $\lambda_{exc} = 300$ nm (black line), $\lambda_{exc} = 405$ nm (red line), $\lambda_{exc} = 490$ nm (blue line); $\lambda_{em} = 430$ nm (black line), $\lambda_{em} = 480$ nm (red line), $\lambda_{em} = 550$ nm (blue line).

differently from the other solid phases, an increased autoabsorption phenomenon by increasing the particles dimension cannot be totally excluded for TTPyr(HT).

To acquire more information on the emissive behavior, amorphous films (XRPD evidence, see Figure S52) were prepared by melting (at 300 °C) powders of TTPyr and rapidly quenching the melt with liquid nitrogen. The film shows an intense fluorescence at 465 nm (much lower energy with respect to that of the PMMA blended film) and a hardly visible

phosphorescence (534 nm) appearing only by exciting at low energy (Table 1 and Figures 10 left and S45). The excitation spectrum monitored at 470 nm is characterized by well separated absorption peaks at 265, 310 and 390 nm which are red shifted with respect to those observed in solution. Moreover, neat films prepared by casting of a DCM solution of TTPyr show the same absorption and emissive behavior ($\Phi = 50\%$, Figure 10 right), comprising one broad fluorescence (at 470 nm) and one phosphorescence (510 nm) selectively activated by exciting at low energy. By heating the cast films at 220 °C for 30 and 90 minutes, a quenching of the emission ($\Phi = 12\%$), a very small blue shift of the fluorescence (at 459 nm) and a red shift of the phosphorescence (at 547 nm) are observed, together with a broadening of the bands in the excitation spectrum, which becomes very similar to those of crystals including the low energy tail at about 450 nm. A more efficient ISC and a stabilization of the triplet through thermal annealing are suggested by the measured lifetimes of the two emissive components (6.95 ns and 4.78 ms versus 1.73 ns and 13.63 ms for the pristine and annealed cast film, Figures S46, S47 and S48, S49, respectively).

The absorption red shift induced by intermolecular interactions is supported by DFT/TDDFT calculations on prototype dimeric models of TTPyr in TTPyr(RT) and TTPyr(HT), obtained by optimizing the geometry of two interacting molecules extracted from the respective crystal structures. Compared with the isolated monomer, conformation of the molecules in the TTPyr(RT) dimer is much less twisted as indicated by their τ_{opt} values, which vary from 110.3° (monomer) to 126.8° and 123.9° (dimer), approaching the corresponding X-ray value ($\tau_{cryst} = 128.9°$). On the other hand, τ_{opt} of the TT-Pyr(HT) dimer undergoes only a slight decrease (from 67.4° to 59.2° and 63.2°) because in the isolated dimer the pyrene moiety is still free to get the minimum energy conformation, differently from what it happens in the crystal structure ($\tau_{cryst} = 48.8°$). As a result, S_1 of the TT-Pyr(HT) dimer is essentially unvaried with respect to the monomer, while for the TTPyr(RT) dimer the S_1 level and its relaxed value, computed at 316 and 396 nm respectively, are both red shifted with respect to the values of the monomer (304 and 384 nm, respectively), in agreement with the experimental data.

To conclude, the emissive behavior of TT-Pyr in different phases can be summarized as follows: i) the chromophore frozen in PMMA assumes the minimum energy conformation, $S_{0,HT}$, giving the higher energy fluorescence from $S_{1,HT}$; ii) in solution, the flatness of the S_0 PES is responsible for a broad fluorescence emission coming from two states, $S_{1,HT}$ and $S_{1,RT}$; iii) in TTPyr(RT), TTPyr(Et) and TTPyr(Me) crystals, characterized by strong π-π intermolecular interactions involving both TT and Pyr moieties, the chromophore is rigidified in the $S_{0,RT}$ minimum. This results in the observation of only the low energy fluorescence from $S_{1,RT}$; iv) in TTPyr(HT) the crystalline arrangement, where only the TT moieties are strongly mutually interacting, allows some conformational freedom to the Pyr moiety, so that both emissions from $S_{1,HT}$ and $S_{1,RT}$ are observed; v) for all phases, an easier ISC to a triplet state is observed for greater crystals, proven by the longer fluorescence lifetimes in
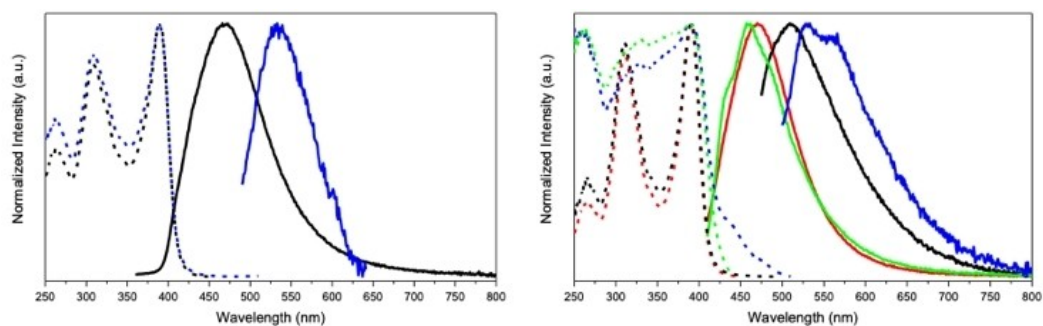
Chemistry–A European Journal

Full Paper
doi.org/10.1002/chem.202102839

Chemistry Europe
European Chemical
Societies Publishing

Figure 10. Normalized emission (full line) and excitation (dashed line) spectra at RT. Left: TTPyr amorphous film $\lambda_{exc} = 340$ nm (black line), $\lambda_{exc} = 470$ nm (blue line); $\lambda_{em} = 470$ nm (black line), $\lambda_{em} = 534$ nm (blue line). Right: TTPyr cast film. Pristine: $\lambda_{exc} = 390$ nm (red line), $\lambda_{exc} = 460$ nm (black line); $\lambda_{em} = 470$ nm (red line), $\lambda_{em} = 514$ nm (black line). Heated 90 min at 220 °C: $\lambda_{exc} = 390$ nm (green line), $\lambda_{exc} = 480$ nm (blue line); $\lambda_{em} = 458$ nm (green line), $\lambda_{em} = 530$ nm (blue line).

ground samples. This may be explained by the expected more extended intermolecular interactions in large crystals.[36,37] Moreover, a stabilization of the triplet state is observed in large TTPyr(HT) aggregates; vi) in the amorphous film the most peculiar feature is the high resolution of the excitation spectrum, which suggests the presence of very small aggregates, producing a broad fluorescence and a very weak phosphorescence. The former due to both conformations, as in solution, the latter due to intermolecular interactions which partially inhibit non-radiative deactivation channels competitive with phosphorescence; vii) this behavior is maintained in pristine cast film where only small aggregates are present. By thermal treatment at 220 °C, the obtained bigger aggregates are probably to be correlated with the more thermodynamically stable conformation ($S_{0,HT}$) of TTPyr(HT), in agreement with intensification of the high energy fluorescence, shortening of the fluorescence lifetimes and lengthening of the phosphorescence lifetimes.

Biological tests

The special luminescent properties of TTPyr aggregate materials could possess huge potential in biological imaging due to their long-lived emission, tunable emission range and high quantum yields in all phases. On the other hand, triazinic functionalities are frequently used in the biological field[38] due to their ability to work as central scaffold for further modification or as mimetic of purine moieties.[39] Therefore, we assumed that the insertion of the TT moiety on pyrene dyes could, not only modify its photophysical properties, but also enhance the biological value acting as a carrier through the cell membrane. To this aim, the aggregation-induced emission property of TTPyr was investigated by adding increasing amounts of non-solvent water to a DMSO solution of the chromophore keeping the concentration equal to 10^{-5} M (Figure 11). By irradiating such suspensions at 340 nm, a gradual increase and a concomitant blue shift of the emission from 420 to 400 nm is observed by increasing the water fraction up to 70% (water content in volume). Further water addition results in an attenuation of this emission. Moreover, the appearance of an additional low energy component at about 480 nm is observed for the 90% and 99% suspension (Figure 12). At 405 nm excitation wavelength, the intensification of the low energy component can be monitored since freed from the more intense high energy one. It is thus evident that the 480 nm emission is already visible and actually more intense at 80% water content.
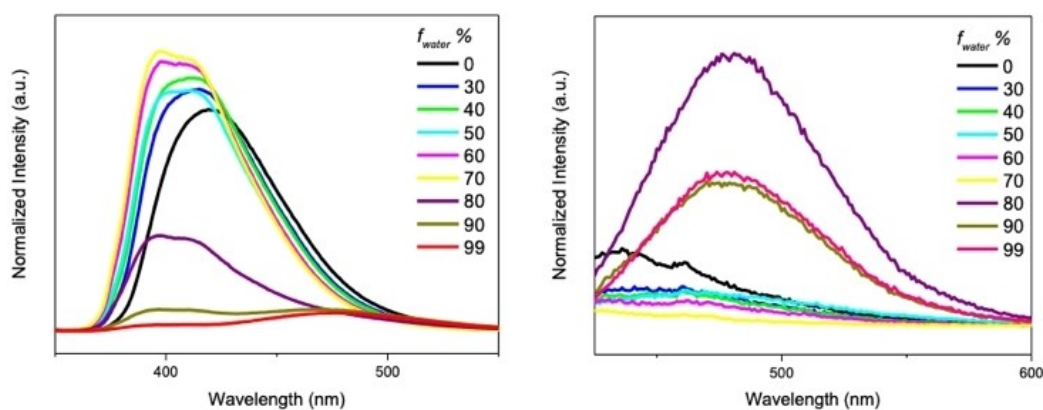

Figure 11. Emission spectra of TTPyr (10^{-5} M) in DMSO/H_2O mixtures with different water fractions (f_w) at RT. Left: $\lambda_{exc} = 340$ nm, right: $\lambda_{exc} = 405$ nm.
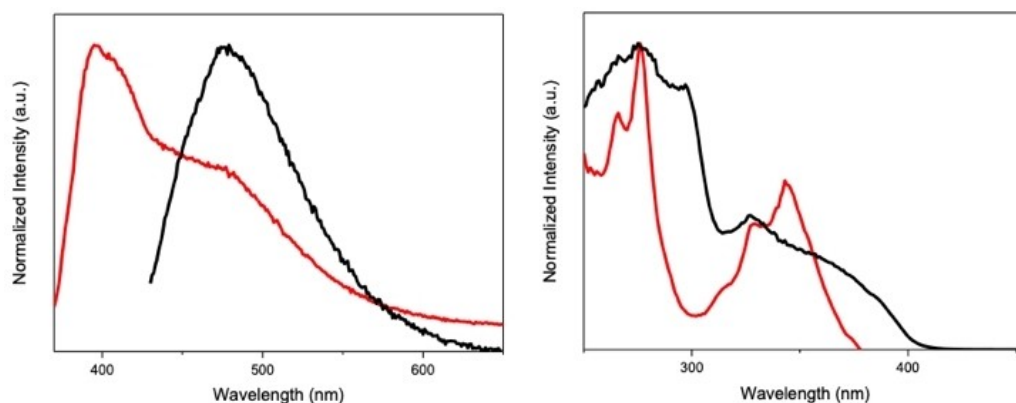
Chemistry–A European Journal

Full Paper
doi.org/10.1002/chem.202102839

Chemistry
Europe
European Chemical
Societies Publishing

Figure 12. TTPyr aggregates in DMSO/H$_2$O (10/90 v/v) 10^{-5} M at RT. Left: Normalized emission spectra of $\lambda_{exc} = 346$ nm (red line); $\lambda_{exc} = 405$ nm (black line); right: Normalized excitation spectra $\lambda_{em} = 398$ nm (red line); $\lambda_{em} = 480$ nm (black line).

Time resolved experiment on the 90% water containing suspension reveals the fluorescence nature of the 480 nm emission ($\tau_{av} = 25.66$ ns, Figure S51), which must be correlated to the aggregate species, similarly to what observed for pristine cast films. The emission peak at 480 nm appears to be suitable for the bacteria and cell imaging as reported below.

Cell experiments were carried out to investigate the subcellular location behaviors of TTPyr aggregates. The results indicate that TTPyr aggregates are detectable inside eukaryotic (HeLa and HLF) cells through confocal laser scanning microscopy (CLSM) at concentration as low as 10 μM. To determine the location of TTPyr, colocalization experiments were con-

ducted. As shown in Figures 13 and 14 (HeLa cells) and Figures S53 and S54 (HLF cells), signals from TTPyr aggregates partially overlap with those of the lysosomes and lipid droplets, a result to be potentially ascribed to the hydrophobic nature of TTPyr. On the other hand, only a partial overlap between TTPyr and mitochondria signals is observed. Moreover, in situ steady state spectrum shows a perfect match with that obtained with the 90% non-solvent aggregate, confirming the presence of TTPyr inside the cells (Figure S55). These results indicate that TTPyr can easily enter the cell and locate at various organelles where important cellular processes occur. Moreover, TTPyr can also stain bacteria. As shown in Figure S56, TTPyr can stain with
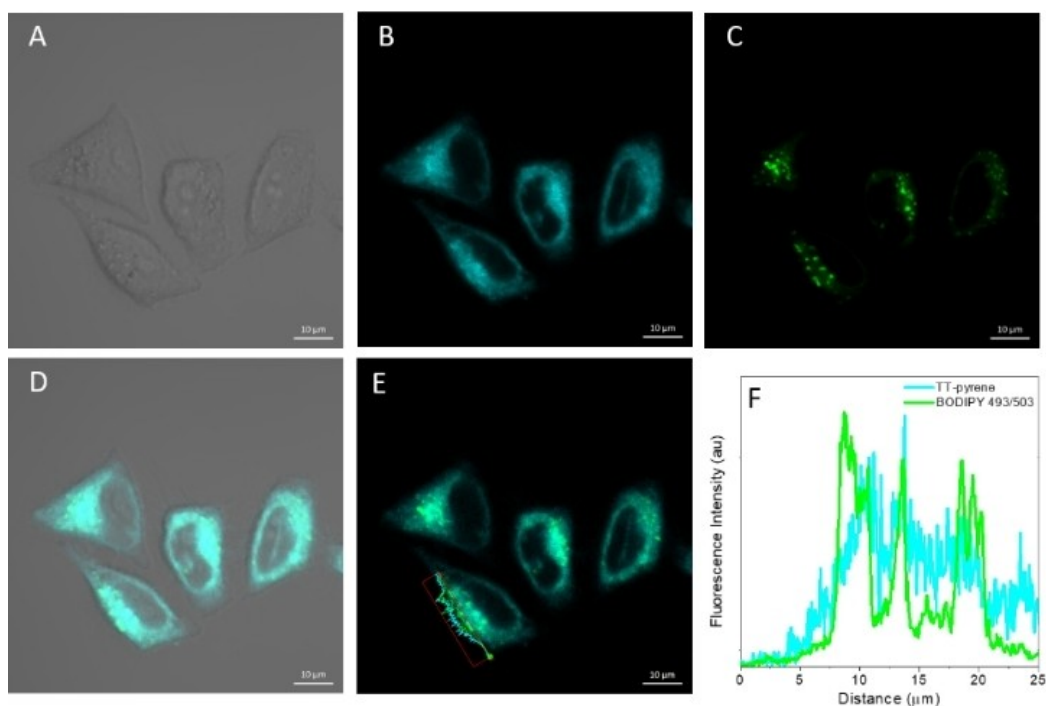

Figure 13. HeLa cells co-staining experiment. A) MitoTracker Deep Red. B) LysoTracker Green DND 26. C) TTPyr 10 μM. D) Bright field. E) On screen axial fluorescent intensity of TTPyr, MitoTracker and LysoTracker. F) The fluorescence intensities of MTDR, LTG, TTPyr along the axis.
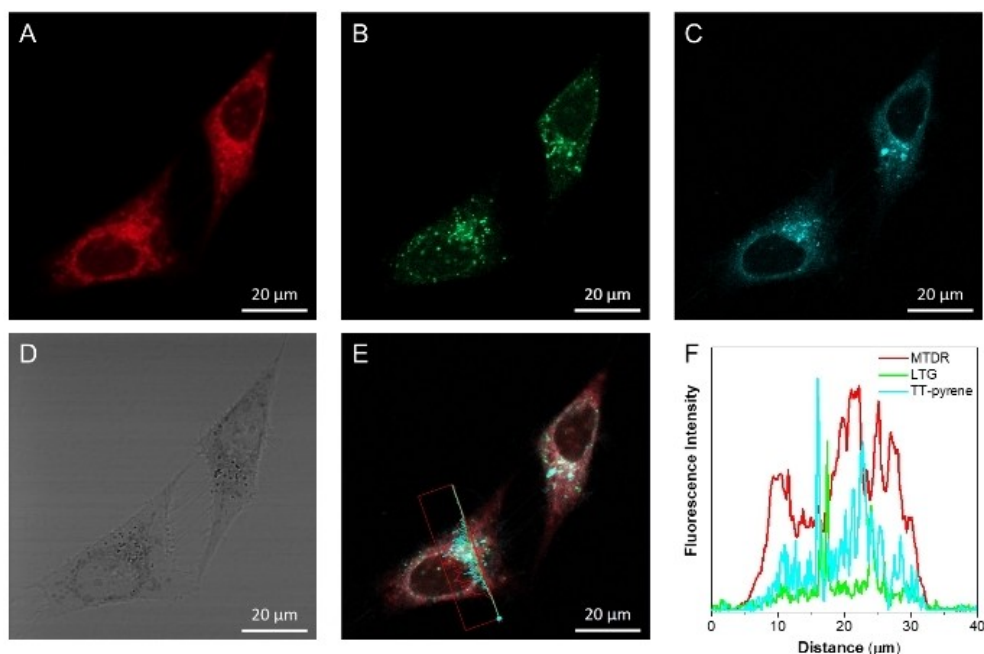
Chemistry–A European Journal

Full Paper
doi.org/10.1002/chem.202102839

Chemistry Europe
European Chemical
Societies Publishing

Figure 14. HeLa cell co-staining experiment. A) Bright field. B) TTPyr 10 μM. C) BODIPY 493/503. D) Merged image of A—C. E) On screen axial fluorescent intensity of TTPyr and BODIPY 493/503. F) The fluorescence intensities of TTPyr and BODIPY 493/503 along the axis.

high efficiency both *S. aureus* and *E. coli* within 60 min by entering the bacterial cells.

These results indicate that TTPyr can enter both eukaryotic and prokaryotic cells at low concentration in an appropriate time window, making it a suitable probe for sensing of intracellular environment change. More detailed information is expected to be obtained from the long-lived emission of TTPyr.

Biocompatible properties of TTPyr have been measured by using a MTT assay (Figure S57). TTPyr displays distinct cytotoxicity towards cancers other than normal cells. At 10 μM concentration, around 70% of HeLa cells are killed by TTPyr. As reported above, triazinic functionalities are frequently used in the biological field due to their ability to work as central scaffold for further modification or as mimetic of purine moieties.[39] Together with specific drug carriers, TTPyr could potentially be applied as a luminescent drug for anticancer studies.

Conclusion

Two solvate (methanol and ethanol) and two solvent free crystalline forms of TTPyr were isolated and characterized through X-ray diffraction and thermal analysis. Three of them were obtained at room temperature from different solvent mixtures, and one was isolated only at high temperature through a melt crystallization process. The three room-temperature forms are characterized by similar torsional angle between the two flat TT and Pyr fragments and by a quite similar columnar antiparallel arrangement of the molecules which interact through hetero TT/Pyr stacking. Interestingly, the high

temperature form, TTPyr(HT), shows different conformation of the molecule and a complete different molecular packing in which only homo TT/TT stacking is evident. The TTPyr(HT) form, once formed, remains stable at RT and shows a melting point which is about 60 °C higher than that of the RT solvent free form. Moreover, TTPyr(HT), the only member of the TT family belonging to a non-centrosymmetric space group, possesses an SHG efficiency 10 times that of standard urea.

The photophysical results reported for TTPyr in different phases and polymorphs has allowed first of all to highlight the high performance (high quantum yield) of this dye regardless its physical status, which makes the compound an appealing resource in view of different applications. Bioimaging experiments indicate that TTPyr could enter cells easily and locate at cytoplasm of cells. Moreover, solid samples reveal RTP and dual fluorescence which can be tuned through grinding and crystallization procedures. Such behavior has been interpreted on the basis of the conformational freedom shown by the dye in the ground state, as supported by DFT/TDDFT calculations.

In view of the good results obtained with pyrene, cyclic triimidazole could be introduced as substituent on other flat scaffolds in order to switch on or to enhance phosphorescent emissions.

Supporting Information

Synthetic details, NMR and mass spectra, thermal analyses, details of the crystal structure determinations, photoluminescence measurements, biological tests and computational details are provided in the supporting Information. Deposition Number

Chemistry–A European Journal

Full Paper
doi.org/10.1002/chem.202102839

Chemistry
Europe
European Chemical
Societies Publishing

Acknowledgements

Conflict of Interest

The authors declare no conflict of interest.

[1] W. Qin, P. Zhang, H. Li, J. W. Y. Lam, Y. Cai, R. T. K. Kwok, J. Qian, W. Zheng, B. Z. Tang, *Chem. Sci.* **2018**, *9*, 2705–2710.
[2] J. Zhi, Q. Zhou, H. Shi, Z. An, W. Huang, *Chem. Asian J.* **2020**, *15*, 947–957.
[3] L. Gu, H. Wu, H. Ma, W. Ye, W. Jia, H. Wang, H. Chen, N. Zhang, D. Wang, C. Qian, Z. An, W. Huang, Y. Zhao, *Nat. Commun.* **2020**, *11*, 944.
[4] Y. Lei, W. Dai, J. Guan, S. Guo, F. Ren, Y. Zhou, J. Shi, B. Tong, Z. Cai, J. Zheng, Y. Dong, *Angew. Chem. Int. Ed.* **2020**, *59*, 16054–16060.
[5] R. Gao, D. Yan, *Chem. Commun.* **2017**, *53*, 5408–5411.
[6] S. Hirata, K. Totani, H. Kaji, M. Vacha, T. Watanabe, C. Adachi, *Adv. Opt. Mater.* **2013**, *1*, 438–442.
[7] Z. An, C. Zheng, Y. Tao, R. Chen, H. Shi, T. Chen, Z. Wang, H. Li, R. Deng, X. Liu, W. Huang, *Nat. Mater.* **2015**, *14*, 685–690.
[8] E. Lucenti, A. Forni, C. Botta, L. Carlucci, C. Giannini, D. Marinotto, A. Previtali, S. Righetto, E. Cariati, *J. Phys. Chem. Lett.* **2017**, *8*, 1894–1898.
[9] E. Lucenti, A. Forni, C. Botta, L. Carlucci, C. Giannini, D. Marinotto, A. Pavanello, A. Previtali, S. Righetto, E. Cariati, *Angew. Chem. Int. Ed.* **2017**, *56*, 16302–16307.
[10] X.-K. Ma, Y. Liu, *Acc. Chem. Res.* **2021**, *54*, 3403–3414.
[11] R. Kabe, C. Adachi, *Nature* **2017**, *550*, 384–387.
[12] D. Li, F. Lu, J. Wang, W. Hu, X. M. Cao, X. Ma, H. Tian, *J. Am. Chem. Soc.* **2018**, *140*, 1916–1923.
[13] Z. Y. Zhang, W. W. Xu, W. S. Xu, J. Niu, X. H. Sun, Y. Liu, *Angew. Chem. Int. Ed.* **2020**, *59*, 18748–18754.
[14] M. Hayduk, S. Riebe, J. Voskuhl, *Chem. Eur. J.* **2018**, *24*, 12221–12230.
[15] M. Baroncini, G. Bergamini, P. Ceroni, *Chem. Commun.* **2017**, *53*, 2081–2093.
[16] L. Sun, W. Zhu, F. Yang, B. Li, X. Ren, X. Zhang, W. Hu, *Phys. Chem. Chem. Phys.* **2018**, *20*, 6009–6023.
[17] O. Bolton, K. Lee, H.-J. Kim, K. Y. Lin, J. Kim, *Nat. Chem.* **2011**, *3*, 205–210.
[18] H. Shi, Z. An, P.-Z. Li, J. Yin, G. Xing, T. He, H. Chen, J. Wang, H. Sun, W. Huang, Y. Zhao, *Cryst. Growth Des.* **2016**, *16*, 808–813.
[19] Z. Lin, R. Kabe, N. Nishimura, K. Jinnai, C. Adachi, *Adv. Mater.* **2018**, *30*, 1803713.
[20] E. Lucenti, A. Forni, C. Botta, L. Carlucci, A. Colombo, C. Giannini, D. Marinotto, A. Previtali, S. Righetto, E. Cariati, *ChemPhotoChem* **2018**, *2*, 801–805.
[21] E. Lucenti, A. Forni, C. Botta, C. Giannini, D. Malpicci, D. Marinotto, A. Previtali, S. Righetto, E. Cariati, *Chem. Eur. J.* **2019**, *25*, 2452–2456.
[22] C. Giannini, A. Forni, D. Malpicci, E. Lucenti, D. Marinotto, A. Previtali, L. Carlucci, E. Cariati, *Eur. J. Org. Chem.* **2021**, *2021*, 2041–2049.
[23] A. Previtali, E. Lucenti, A. Forni, L. Mauri, C. Botta, C. Giannini, D. Malpicci, D. Marinotto, S. Righetto, E. Cariati, *Molecules* **2019**, *24*, 2552.
[24] E. Lucenti, A. Forni, A. Previtali, D. Marinotto, D. Malpicci, S. Righetto, C. Giannini, T. Virgili, P. Kabacinski, L. Ganzer, U. Giovanella, C. Botta, E. Cariati, *Chem. Sci.* **2020**, *11*, 7599–7608.
[25] C. K. Ellison, T. N. Dalia, A. Vidal Ceballos, J. C.-Y. Wang, N. Biais, Y. V. Brun, A. B. Dalia, *Nat. Microbiol.* **2018**, *3*, 773–780.
[26] A. Heinrichs, *Nat. Cell Biol.* **2009**, *11*, S7-S7.
[27] R. Yuste, *Nat. Methods* **2005**, *2*, 902–904.
[28] M. Fernández-Suárez, A. Y. Ting, *Nat. Rev. Mol. Cell Biol.* **2008**, *9*, 929–943.
[29] B. Huang, M. Bates, X. Zhuang, *Annu. Rev. Biochem.* **2009**, *78*, 993–1016.
[30] Q. Zhao, C. Huang, F. Li, *Chem. Soc. Rev.* **2011**, *40*, 2508–2524.
[31] S. Gan, J. Zhou, T. A. Smith, H. Su, W. Luo, Y. Hong, Z. Zhao, B. Z. Tang, *Mater. Chem. Front.* **2017**, *1*, 2554–2558.
[32] S. Qi, S. Kim, V.-N. Nguyen, Y. Kim, G. Niu, G. Kim, S.-J. Kim, S. Park, J. Yoon, *ACS Appl. Mater. Interfaces* **2020**, *12*, 51293–51301.
[33] C. Ji, L. Lai, P. Li, Z. Wu, W. Cheng, M. Yin, *Aggregate* **2021**, e39.
[34] H. Gao, X. Ma, *Aggregate* **2021**, e38.
[35] S. K. Kurtz, T. T. Perry, *J. Appl. Phys.* **1968**, *39*, 3798–3813.
[36] G. Chen, S. Guo, H. Feng, Z. Qian, *J. Mater. Chem. C* **2019**, *7*, 14535–14542.
[37] J. Yang, X. Gao, Z. Xie, Y. Gong, M. Fang, Q. Peng, Z. Chi, Z. Li, *Angew. Chem. Int. Ed.* **2017**, *56*, 15299–15303.
[38] L. Wackett, M. Sadowsky, B. Martinez, N. Shapir, *Appl. Microbiol. Biotechnol.* **2002**, *58*, 39–45.
[39] F. P. L. Lim, A. V. Dolzhenko, *Eur. J. Med. Chem.* **2014**, *85*, 371–390.